Available online at www.sciencedirect.com
SCIENCE DIRECT®
Spectrochimica Acta Part B 59 (2004) 689–699
SPECTROCHIMICA ACTA PART B
www.elsevier.com/locate/sab

Characterization and speciation of depleted uranium in individual soil particles using microanalytical methods

S. Török[a,*], J. Osán[a], L. Vincze[b,a], S. Kurunczi[a], G. Tamborini[c], M. Betti[c,1]

[a]KFKI Atomic Energy Research Institute, P.O. Box 49, H-1525 Budapest, Hungary
[b]Department of Chemistry, University of Antwerp, Universiteitsplein 1, B-2610 Antwerpen, Belgium
[c]European Commission, JRC, Institute for Transuranium Elements, P.O. Box 2340, D-76125 Karlsruhe, Germany

Received 3 November 2003; accepted 30 January 2004

Abstract

Microanalytical techniques for elemental composition and nuclide-specific analysis have been used to identify the origin and the leachability of depleted uranium particles. The soil particle samples were collected from Kosovo area a few years after the war, the presence of fine particles with depleted uranium as major component was easily identified by EPMA and SIMS. The ultrafine uranium particles were often attached to larger soil particles and contained Ti and Al, being typical components of the penetrator and its cladding. The oxidation state of uranium in the single particles was measured by micro-XANES and found to be in the less soluble form IV while every particle contained a small fraction of mobile uranium VI as well.

Keywords: μ-X-ray fluorescence; μ-XANES; EMPA; Scanning electron microscopy; Secondary ion mass spectrometry; Depleted uranium; Microparticles

1. Introduction

Depleted uranium (DU) is the by-product in the production of enriched uranium for civil uses (nuclear fuels). If as feed material for the enrichment reprocessed uranium is employed, DU can contain traces of minor actinides and fission products [1]. Due to its physical properties (e.g. high density that is about twice that of lead) it finds applications for civil and military uses. For instance, it is used in counterweights or ballast in aircraft; radiation shield in medical equipment; as containers for the transport of radioactive material and chemical catalyst [2]. The Boeing 747-258F that crashed into a block of flats in Amsterdam in October 1992 carried 282 kg of DU counterweights. The Boeing-747 crashed near Stansted airport in England in January 2000, was estimated to be carrying ca. 425 kg of DU counterweights [3]. As for military applications, it is used in munitions designed to penetrate armor plate and is also used to reinforce military vehicles such as tanks. DU munitions have been used during the Gulf War, in Bosnia Herzegovina and in Kosovo conflicts. Following the use of depleted uranium ammunitions during these conflicts, concerns over the health of personnel who were exposed to DU have received international attention from the media. The concerns relate to instances where persons exposed to DU are purported to exhibit various forms of morbidity soon after exposure [4]. The general assumption is that the cause is related to the radiotoxicity of DU; this is unlikely, as the latent period between exposure and the onset of disease, such as cancer or leukemia, is typically 7–10 years [4]. Moreover, DU is approximately 40% less radioactive than natural uranium, and the concern for human exposure is its chemical rather than its radiological toxicity [4,5]. Priest presents a comprehensive review of why DU cannot be linked to the leukemia and cancer [6].

The major risk is DU dust. In fact, the disintegration of a DU shell on impact is associated with high temperature effects, the production of fragments as shrapnel and finely divided particulate matter as a consequence of volatilization processes. Both civilian

*Corresponding author. Fax: +36-1-392-2299.
E-mail addresses: sztorok@sunserv.kfki.hu (S. Török), betti@itu.fzk.de (M. Betti).
[1] Also corresponding author.

0584-8547/04/$ - see front matter © 2004 Elsevier B.V. All rights reserved.
doi:10.1016/j.sab.2004.02.003

and military employment of DU can produce aerosol that generates uranium-bearing microparticles. Therefore, a dispersion and redeposition of these microparticles in the environment can occur. Depending on aerosol speciation, inhalation may lead to a protracted exposure of the lung and other organs. After deposition on the ground, resuspension can take place if the DU containing particle size is sufficiently small. In order to understand transport and dispersion mechanisms of DU such as weathering rates, mobilization and biological uptake, of microparticles containing DU, it is important to determine the oxidation state of uranium in the microparticles. In this paper, the results obtained when studying uranium particles as found in two soil samples stemming from Kosovo environment, in terms of particle size, elemental chemical composition, uranium isotopic content and oxidation states are reported.

2. Materials and methods

2.1. Samples

Soil samples collected by the UNEP expedition conducted in September 2000 in the Kosovo area were examined for DU containing particles. The samples investigated consisted of two soil specimens collected at 0–5-cm depth. After collection, the samples were dried, homogenized and sieved at the IAEA analytical laboratories of Seibersdorf. For the investigation here reported, the particles were suspended in *n*-hexane containing rubber cement, then filtered through a Nuclepore membrane filter. Rubber cement was found to be an ideal fixing material containing trace elements in very low concentration in low-Z element matrix and providing elastic fixing. In order to break large particle agglomerations into individual particles, the suspension was subjected to ultrasonic vibration.

In order to obtain a detailed size distribution of the uranium-rich particles and for pre-selection of particles for secondary ion mass spectrometry (SIMS) analysis, several sub-samples for each soil sample were dispersed on high purity carbon planchets (Fullam Inc., grade A carbon planchets No. 17680). Pressed soil pellets were also prepared for measurements.

2.2. SEM measurements

The analyses of particles prepared on Nuclepore filters were performed using a PHILIPS 505 scanning electron microscope (SEM) equipped with a Link EDX detector. The detector has a 7.62-μm thick beryllium window, and its energy resolution is 150 eV at 5.9 keV. The EPMA measurements were carried out at an accelerating voltage of 20 kV, and a beam current of 1 nA. The single particles were measured automatically, controlled by a homemade computer software, only scanning the electron beam over the whole projected area of the particles. Approximately 300 particles were measured in each sample. Morphological parameters such as diameter and shape factor were calculated using the image processing routine of the measuring program. The characteristic X-ray spectra obtained from the particles have been evaluated by non-linear least squares fitting, using the AXIL code [7]. Based on the data set obtained, the particles were further classified using hierarchical cluster analysis (HCA). The calculations were performed using the statistical software package IDAS [8].

The particle distribution on the carbon planchets was mapped by a SEM (RJL Micro&Analytics GmbH) and the co-ordinates recorded for further transfer to the SIMS instrument, where the isotopic characterization of particles was performed.

To search for uranium containing particles, the samples were scanned automatically using the backscattered mode. The applied voltage was 30 kV. The contrast was set so that only particles containing elements with high atomic number (Z) were detected. They appear as bright spots against an otherwise dark background signal. Whenever such a signal is received from the sample, a particle is identified and the system analyses it by taking the X-ray spectrum with the EDX detector for 3 s. The obtained energy spectrum is automatically evaluated by comparing the peaks in the spectrum with known peaks in the source library. Particles are regarded as uranium-rich if their uranium content is more than 40%. From these analyses, the number of uranium particles on the planchet (support), together with their elemental composition as well as the co-ordinates are obtained.

2.3. SIMS measurements

A CAMECA IMS 6f secondary ion mass spectrometer (SIMS) at the Institute for Transuranium Elements was used. This instrument consists of a double-focusing mass spectrometer that allows fast switching between the masses. In addition, it has microfocus ion sources (caesium and duoplasmatron with oxygen or argon gas) that can be used either in the microscope or microprobe mode. The instrument is also equipped with a spatially resolved pulse-counting resistive anode encoder (RAE) used for mapping the entire sample surface. The SIMS was employed both in the microscope and microprobe modes [9].

In the measurements, the samples were bombarded with a primary O_2^+ beam of 15 keV ($\pm 0.5\%$) with a current intensity between 1 and 2 nA and a diameter of 3–5 μm. Positive secondary ions were accelerated to 5 keV and intensities were controlled by the tuning of the primary ion beam current. The energy window was adjusted between 40 and 50 eV to reduce molecular ion contributions. The instrument can typically operate with a mass resolving power (MRP) of 10 000. However,

Table 1
Result of cluster analysis for the (a) Kosovo 1 and (b) Kosovo 4 samples

(a)

Kosovo 1	Clust 1	Clust 2	Clust 3	Clust 4	Clust 5	Clust 6	Clust 7	Clust 8	Clust 9	Clust 10
Abundance (%)	39.7	9.9	9.3	9.0	7.6	7.6	7.3	4.1	3.2	2.3
Diameter (μm)	2.5	1.6	2.1	2.8	1.9	3.4	2.3	2.8	1.7	0.8
Element	Normalized X-ray intensity (%)									
Al	21.5	14.7	14.9	9.6	21.3	17.4	8.8	21.5	17.2	9.4
Si	26.6	20.3	20.2	13.1	27.9	40.3	14.8	32.9	55.3	17.8
P	1.1	7.0	0.2	0.0	0.0	1.1	0.0	0.7	0.6	0.0
S	0.6	8.3	0.9	0.1	0.6	0.8	0.0	0.0	0.0	0.0
Cl	0.1	5.2	0.1	0.0	0.0	0.1	0.0	0.0	0.0	0.0
K	8.9	5.2	6.5	11.1	0.4	4.9	0.0	18.5	0.4	10.6
Ca	14.0	5.9	35.6	49.3	15.2	11.5	54.8	7.9	7.3	2.3
Ti	3.2	1.2	0.8	0.1	1.5	0.9	0.0	0.9	0.0	2.4
Cr	0.2	1.4	0.3	0.2	0.0	0.4	0.5	0.0	0.0	5.2
Mn	1.7	1.9	0.4	0.1	0.6	0.4	0.0	0.2	0.0	2.9
Fe	12.1	6.2	7.4	4.4	13.3	7.7	3.1	6.3	4.6	8.3
Ni	0.1	0.8	0.1	0.1	0.0	0.1	0.0	0.0	0.0	4.5
Cu	5.3	10.3	6.7	6.3	9.8	7.6	9.9	6.3	7.9	18.2
Zn	4.4	8.4	5.5	5.3	8.2	6.4	8.2	4.8	6.7	14.8
Zr	0.0	0.0	0.0	0.0	0.0	0.0	0.0	0.0	0.0	0.0
Pb	0.1	2.2	0.5	0.2	0.2	0.3	0.0	0.1	0.0	3.2
U	0.1	1.1	0.0	0.1	1.1	0.2	0.0	0.1	0.0	0.5

(b)

Kosovo 4	Clust 1	Clust 2	Clust 3	Clust 4	Clust 5	Clust 6	Clust 7	Clust 8	Clust 9	Clust 10
Abundance (%)	26.2	18.4	15.5	13.3	8.7	8.7	4.9	1.9	1.6	0.6
Diameter (μm)	1.8	2.5	2.5	2.6	2.1	2.1	0.9	1.3	3.8	3.0
Element	Normalized X-ray intensity (%)									
Al	21.0	11.4	15.7	9.0	17.9	19.8	14.6	11.3	11.9	0.0
Si	27.2	15.7	21.2	12.4	47.3	25.3	21.0	20.5	14.2	0.0
P	0.2	0.3	0.1	0.1	0.1	0.0	4.1	0.0	0.0	0.0
S	0.3	0.5	0.1	0.1	0.2	0.0	2.9	0.0	0.0	0.0
Cl	0.0	0.2	0.0	0.1	0.0	0.0	2.3	0.0	0.0	0.0
K	10.0	8.0	8.9	10.2	4.6	10.4	5.3	0.0	5.0	18.4
Ca	15.4	45.0	33.6	51.8	12.7	23.5	15.8	42.1	23.0	21.3
Ti	2.7	0.7	0.4	0.2	0.2	1.5	1.6	0.0	6.5	14.5
Cr	0.1	0.1	0.1	0.2	0.0	0.0	0.6	0.0	0.0	0.0
Mn	1.1	0.1	0.2	0.3	0.1	0.3	1.0	0.0	1.3	0.0
Fe	12.1	6.4	8.6	3.8	6.7	9.9	4.4	0.0	27.0	5.4
Ni	0.0	0.0	0.0	0.0	0.0	0.0	0.9	0.0	0.0	0.0
Cu	5.3	6.2	6.2	6.7	5.5	5.4	12.5	14.6	6.2	15.1
Zn	4.4	4.9	5.0	5.3	4.5	4.1	9.5	11.5	5.0	11.1
Zr	0.0	0.0	0.0	0.0	0.0	0.0	0.6	0.0	0.0	0.0
Pb	0.0	0.3	0.0	0.0	0.1	0.0	1.3	0.0	0.0	0.0
U	0.1	0.2	0.0	0.0	0.0	0.0	1.6	0.0	0.0	14.3

Average composition (in normalized X-ray intensity), average diameter and abundance of the obtained 10 clusters are presented. The clusters are listed in descending order of abundance.

for the measurements of uranium and plutonium isotopes, a MRP of 1000 is sufficient. With this resolution, flat-top peaks were obtained, which improve the accuracy of the measurements. A detection limit in the range ng/g–pg/g is achieved by optimizing different instrumental parameters, such as acquisition time. The ions were counted with an electron multiplier in the ion counting mode. The combination of the electron multiplier and Faraday cup provides a very high dynamic range for the secondary intensity measurements. The Faraday cup and electron multiplier are used to measure the count rates in the range 5×10^5–5×10^9 c/s and 10^{-1}–10^6 c/s, respectively. The overlap of the intensity range allows combining both detectors within a given analysis.

As for uranium isotopic composition, the mass calibration on the masses 234, 235, 236 and 238 was performed before starting a new sample or a new cycle

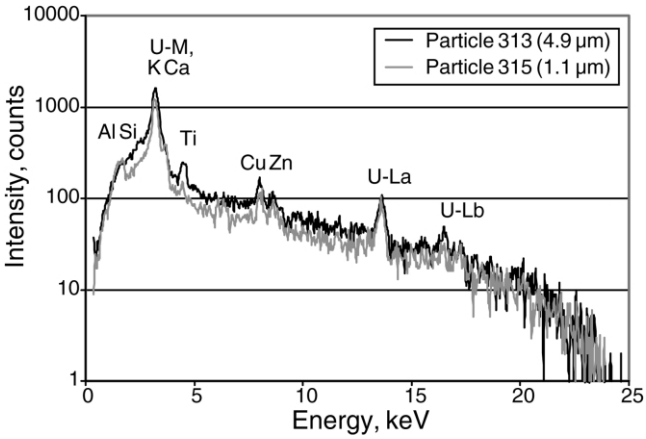

Fig. 1. SEM/EDX spectra of two uranium-rich particles found in the Kosovo 4 soil sample.

of measurements. It was observed that during the course of the day the mass calibration did not change as much as in other mass spectrometric techniques [10,11]. To search for uranium particles, the mass spectrometer was set to mass 235 or 238. The microprobe mode was used, and areas of 250×250 μm on the sample surface were rastered to obtain a mapped distribution of the particles of interest. Once the particles were detected, the primary beam was focused on a single uranium particle and the isotope ratios ($^{234}U/^{238}U$, $^{235}U/^{238}U$, $^{236}U/^{238}U$) were calculated from the measured count rates of the different uranium isotopes.

2.4. Micro-XRF measurements

The SR-based measurements were carried out at D09B-XRF beamline of the National Synchrotron Radiation Laboratory (LNLS) in Campinas, Brazil [12]. The working conditions for the LNLS synchrotron source are: 1.37 GeV electron energy, 175 mA maximum current, and 15 h lifetime. During our measurement, 100 mA and 8 h lifetime were typical. Micro-fluorescence measurements were performed using the white X-ray beam originating from the bending magnet. The 20 μm beam size on the sample was determined by a tapered glass capillary. Micromatter thin film standards (CdSe, Pb, SmF_3, Sr, TmF_3, UF_4, Zn) were used for sensitivity determination.

2.5. Micro-XANES measurements

The experiments were performed at the micro-fluorescence beamline L at HASYLAB in Hamburg, Germany [13]. The white beam of a bending magnet was monochromatized by a Si(111) double monochromator. A polycapillary half-lens (X-ray Optical Systems) was employed for focusing a beam of 1×1 mm^2 down to a spot size of 15-μm diameter. The absorption spectra were recorded in fluorescent mode, tuning the excitation energy near the L_{III} absorption edge of uranium (17 167 eV) by stepping the Si(111) monochromator. The fluorescence yield was detected at an angle of 90° to the incoming beam using an energy-dispersive HPGe detector. Soil particles taken in the Kosovo war area containing approximately 0.1 wt.% of uranium of 20–40-μm diameter were selected for XANES measurements. UO_2 and U_3O_8 particles as well as a thin UF_4 foil (34 μg cm^{-2}, Micromatter) were used as standards. All measurements were carried out using a 1 eV step size. The measuring time for each point varied from 2 s (standard particles) to 60 s (soil particles).

3. Results and discussion

3.1. Characterization of the contaminated soil by SEM

In order to determine the abundance and composition of the depleted uranium containing particles in the soil samples, automated SEM–EDX analysis was performed on the samples prepared on Nuclepore filters. The samples were prepared in such a way that the particles were spread over the filter surface, and large agglomerates were broken to single particles. The particles to be measured were selected using the backscattered electron signal that is a monotonic function of the average atomic number of the excitation volume. After spectral collection and processing, the particles were classified using HCA, based on the normalized characteristic intensities of the measured elements. Table 1 shows the classification results for the two soil samples collected in Kosovo. The most abundant particle groups contained aluminosilicates with different metal content (Ca, Ti, Mn and Fe) that are typical for soils. Uranium-rich particles were found in the Kosovo 4 sample at an abundance of 0.6% (by number). This particle group has an average

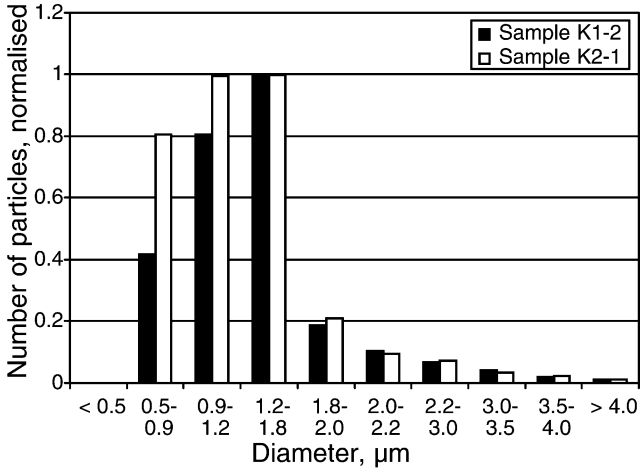

Fig. 2. Size distribution of uranium-rich particles identified in the soil collected from the Kosovo war area.

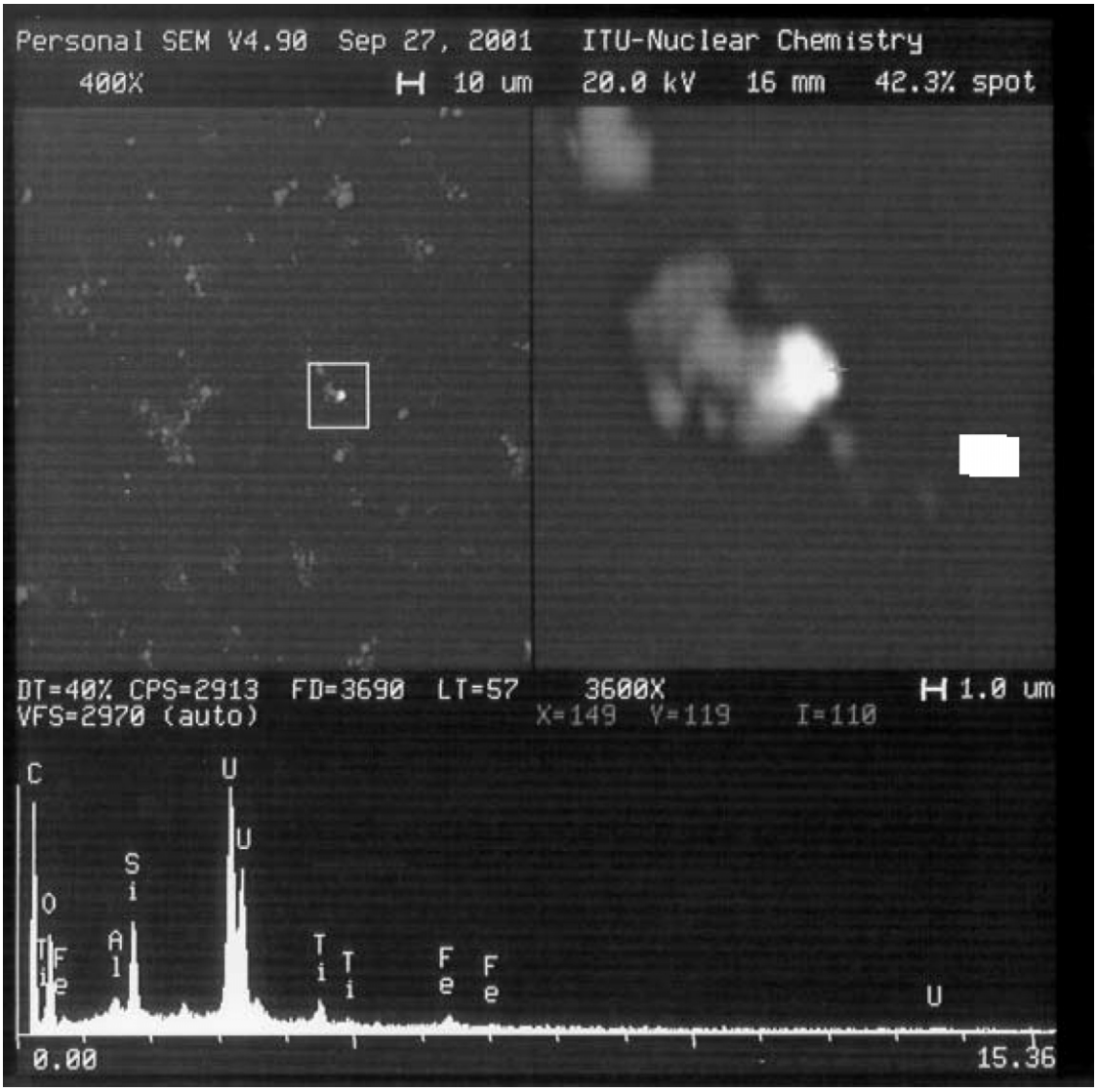

Fig. 3. Backscattered electron images and SEM/EDX spectrum of a uranium-rich particle, showing Al and Ti content.

diameter of 0.8 μm (see Table 1b), indicating the small size of the uranium-rich particles. Typical spectra of two uranium-rich particles are shown in Fig. 1. Submicrometer uranium-rich particles could be agglomerated with soil particles, the abundance of aluminosilicates with approximately 1% uranium content is below 15% for both samples. The average diameter for these groups is between 0.9 and 1.9 μm.

In order to study exclusively the uranium-rich particles, the surface of the pressed soil pellets was measured by SEM/EDX, using a backscattered electron contrast much higher than that of silicon for particle selection. The automatic SEM screening at the surface of the soil sample was performed during 24 h. Several thousands of uranium-rich particles were found, allowing the determination of their size distribution. The particle distribution at the surface of the sample has an average size comprised between 0.5 and 1.8 μm (Fig. 2) in agreement with those found by other authors [14]. However, most of these particles have a mean diameter centered approximately 1 μm. The chemical analysis by EDX revealed the presence of Ti and Al (Fig. 3), elements present in the penetrators and their cladding, respectively.

3.2. SIMS results

The particles localized by the automated SEM with gun shot residue program were then analyzed by SIMS as for uranium isotopic ratios. The results obtained are reported as average values in Tables 2 and 3. They clearly contain DU, and traces of ^{236}U were also detected.

Table 2
Isotopic composition obtained by SIMS, sample 0–5-cm depth

Particle no.	$^{234}U/^{238}U$		$^{235}U/^{238}U$		$^{236}U/^{238}U$		^{234}U		^{235}U		^{236}U		^{238}U	
	Ratio	1σ	Ratio	1σ	Ratio	1σ	wt.%	1σ	wt.%	1σ	wt.%	1σ	wt.%	1σ
1	4.04E−05	1.23E−05	2.18E−03	2.17E−04	3.68E−05	1.76E−05	0.004	0.001	0.215	0.021	0.004	0.002	99.778	0.022
2	4.76E−05	3.06E−05	2.10E−03	2.10E−04	3.37E−05	7.47E−06	0.005	0.003	0.207	0.021	0.003	0.001	99.785	0.021
3	3.54E−05	2.70E−05	2.17E−03	3.15E−04	7.44E−05	3.92E−05	0.003	0.003	0.214	0.031	0.007	0.004	99.775	0.032
4	1.14E−05	9.94E−06	2.10E−03	1.39E−04	3.16E−05	1.59E−05	0.001	0.001	0.207	0.014	0.003	0.002	99.789	0.014
5	8.77E−06	3.98E−06	1.97E−03	1.04E−04	2.64E−05	7.53E−06	0.001	0.000	0.194	0.010	0.003	0.001	99.802	0.010
6	1.12E−05	8.79E−06	1.99E−03	1.36E−04	2.96E−05	1.06E−05	0.001	0.001	0.196	0.013	0.003	0.001	99.800	0.014
7	5.57E−06	3.99E−06	2.05E−03	1.13E−04	3.68E−05	1.33E−05	0.001	0.000	0.202	0.011	0.004	0.001	99.794	0.011
8	<E−06		2.13E−03	1.68E−04	2.85E−05	2.23E−05	<0.001		0.210	0.017	0.003	0.002	99.787	0.017
9	8.32E−06	2.33E−06	1.99E−03	5.78E−05	2.66E−05	4.91E−06	0.001	0.000	0.196	0.006	0.003	0.000	99.800	0.006
10	1.15E−05	7.13E−06	1.98E−03	5.43E−05	4.32E−05	1.64E−05	0.001	0.001	0.195	0.005	0.004	0.002	99.799	0.006
11	4.91E−06	7.49E−06	2.04E−03	1.37E−04	2.46E−05	1.70E−05	0.000	0.001	0.201	0.013	0.002	0.002	99.796	0.014
12	1.07E−05	8.50E−06	2.05E−03	9.98E−05	2.99E−05	2.08E−05	0.001	0.001	0.202	0.010	0.003	0.002	99.794	0.010
Average	1.63E−05		2.06E−03		3.52E−05		0.002		0.203		0.003		99.792	

Table 3
Isotopic composition obtained by SIMS, sample 5–10-cm depth

Particle no.	$^{234}U/^{238}U$		$^{235}U/^{238}U$		$^{236}U/^{238}U$		^{234}U		^{235}U		^{236}U		^{238}U	
	Ratio	1σ	Ratio	1σ	Ratio	1σ	wt.%	1σ	wt.%	1σ	wt.%	1σ	wt.%	1σ
1	1.09E−05	6.30E−06	2.03E−03	1.06E−04	3.60E−05	1.22E−05	0.001	0.001	0.200	0.010	0.004	0.001	99.795	0.011
2	1.46E−05	6.98E−06	2.04E−03	1.51E−04	3.92E−05	1.22E−05	0.001	0.001	0.201	0.015	0.004	0.001	99.794	0.015
3	7.49E−06	8.13E−06	2.04E−03	2.01E−04	3.38E−05	2.50E−05	0.001	0.001	0.201	0.020	0.003	0.002	99.795	0.020
4	2.46E−05	8.26E−06	2.06E−03	1.52E−04	4.60E−05	2.05E−05	0.002	0.001	0.203	0.015	0.005	0.002	99.790	0.015
5	2.21E−05	2.21E−05	1.92E−03	1.93E−04	3.58E−05	2.29E−05	0.002	0.002	0.189	0.019	0.004	0.002	99.805	0.019
6	2.70E−05	1.26E−05	2.03E−03	1.16E−04	6.05E−05	1.54E−05	0.003	0.001	0.200	0.011	0.006	0.002	99.791	0.012
7	4.20E−05	4.13E−05	2.06E−03	4.74E−04	6.47E−05	5.59E−05	0.004	0.004	0.203	0.047	0.006	0.006	99.787	0.048
8	1.57E−05	1.05E−05	2.05E−03	1.26E−04	4.56E−05	1.82E−05	0.002	0.001	0.202	0.012	0.005	0.002	99.792	0.013
9	5.57E−05	3.77E−05	2.16E−03	2.51E−04	1.04E−04	5.60E−05	0.005	0.004	0.213	0.025	0.010	0.006	99.771	0.026
10	1.37E−05	1.46E−05	2.10E−03	1.84E−04	3.40E−05	1.97E−05	0.001	0.001	0.207	0.018	0.003	0.002	99.788	0.018
11	1.80E−05	8.53E−06	2.03E−03	1.49E−04	5.27E−05	2.27E−05	0.002	0.001	0.200	0.015	0.005	0.002	99.793	0.015
12	2.03E−05	1.46E−05	2.08E−03	2.23E−04	6.45E−05	3.73E−05	0.002	0.001	0.205	0.022	0.006	0.004	99.787	0.023
Average	2.27E−05		2.05E−03		5.14E−05		0.002		0.202		0.005		99.791	

As for ^{234}U and ^{236}U, due to the low signal intensity the error is often larger. In general, the total uncertainty on the minor isotopes is decreasing (better counting statistics) when the enrichment increases. The uncertainty on the ^{236}U is significantly higher than that on the ^{234}U, because the 236 intensity is obtained after correction for hydride contribution and the respective errors are propagated into the 236 uncertainty. With such a particle diameter ($\approx$1 μm), the precision that can be achieved is considered the detection limit of the method in these conditions. The signal on mass 239 (due only to the formation of $^{238}UH^+$ molecules) is used to correct the signal on mass 236 for the contribution of $^{235}UH^+$. As for ^{235}U in this case the uncertainty is not strongly depending from the intensity of the signal but from other parameters, e.g. the analysis time.

Table 4
Calculated elemental composition of the soil particles presented in Fig. 4a–c

Elements	Concentration (wt.%)		
	Particle a	Particle b	Particle c
O[a]	47.2	49.2	37.6
Mg[a]	4.7	4.8	3.9
Al[a]	15.3	15.9	11.4
Si[a]	20.5	21.3	17.11
P[b]	0.4	<DL	<DL
S[b]	0.3	<DL	<DL
K[b]	1.6	2.1	7.8
Ca[b]	7.6	2.9	1.7
Ti[b]	0.3	0.5	0.7
V[b]	0.007	0.006	0.02
Cr[b]	0.006	0.01	0.01
Mn[b]	0.03	0.13	0.005
Fe[b]	1.91	2.98	0.09
Co[b]	0.007	<DL	<DL
Ni[b]	0.002	0.004	<DL
Cu[b]	0.002	0.003	0.003
Zn[b]	0.004	0.008	0.002
U[b]	0.13	0.20	18.2

[a]Calculated from EPMA.
[b]Calculated from μ-XRF spectra presented in Fig. 4.
The matrix composition (O, Mg, Al, Si) was assumed as the average composition of soil obtained from electron probe microanalysis. Relative standard deviations are in the range of 2–15%

3.3. The Monte Carlo based quantification scheme for micro-XRF

In the following analytical calculations, a detailed XRF simulation code was used to determine the elemental composition of individual soil particles. For a typical XRF experiment, the simulation code must consider the three most important interaction types in the X-ray energy range of 1–100 keV, i.e. (i) photoelectric absorption followed by X-ray fluorescence or Auger electron emission; (ii) Rayleigh; and (iii) Compton scattering. The simulation of these interactions allows building up the complete spectral response of materials subjected to X-ray excitation in the above mentioned energy range.

Quantification is achieved by iterative adaptation of the simulated elemental concentrations until the deviations between the simulated and experimental peak areas fall within the statistical uncertainties of the recorded fluorescent lines [15].

A significant advantage of the MC simulation based quantification scheme compared to other methods, such as fundamental parameter (FP) algorithms, is that the simulated spectrum can be compared directly to the experimental data in its entirety, taking into account not only the fluorescence line intensities, but also the scattered background of the XRF spectra. This is coupled with the fact that MC simulations are not limited to first or second order approximations and to ideal geometries.

In the past, our MC model has been applied in an iterative manner to quantification of XRF data corresponding to homogeneous or simple heterogeneous sam-

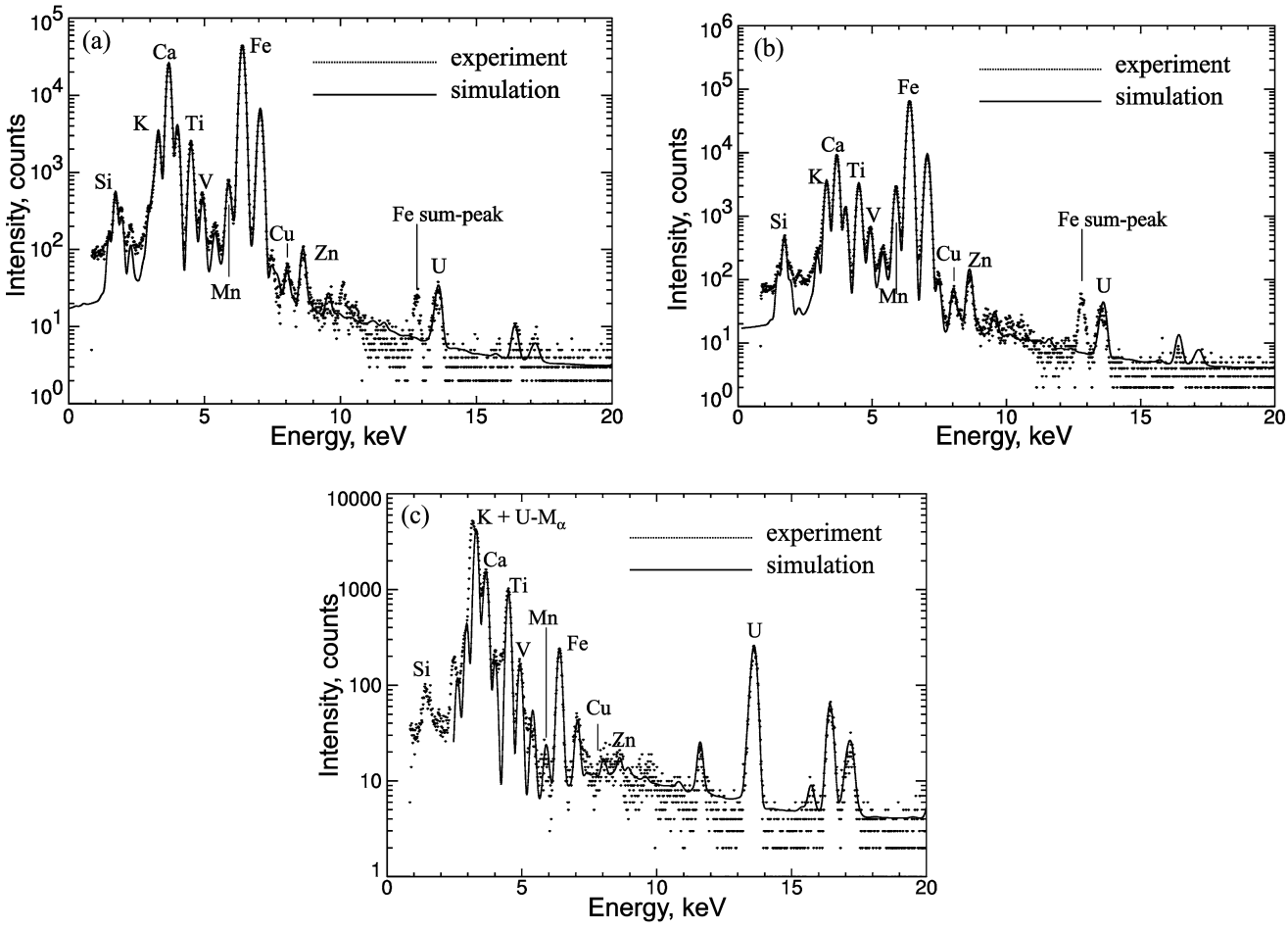

Fig. 4. Comparison of experimental and simulated μ-XRF spectra for three individual soil particles collected from Kosovo. The spectra were collected at LNLS, using white beam excitation.

ples in much the same way as other quantification algorithms based on the fundamental parameter approach. Relative deviations in the range of 2–15% have been achieved by the Monte Carlo quantification scheme, depending on the analyzed element and sample type [16,17]. The use of the code for the quantitative trace-element analysis of individual fly ash particles was previously demonstrated [15].

Errors in the quantitative results are mostly due to the uncertainties in the physical constants (cross sections, fluorescence yields, transition probabilities, etc.) applied in the simulations and due to uncertainties concerning various instrumental parameters. The latter includes uncertainties in the employed excitation spectrum in case of a given polychromatic X-ray source, and often insufficient knowledge on the used detector response function characterizing the energy dispersive detector in the experiment.

3.4. Quantitative analysis of individual soil particles from Kosovo

As the simulation code can predict reliably the measured XRF intensities (and sensitivities) for particulate standards [15], the model could be applied for the quantitative analysis of unknown soil particles originating from Kosovo, based on the iterative adaptation scheme discussed above. As an example, the calculated elemental compositions of three typical individual particles are shown in Table 4, corresponding to particles having elevated U concentrations. In these calculations, the low-*Z* matrix composition (so-called dark-matrix) was estimated by EPMA analysis, based on a Monte Carlo quantification procedure for electron interactions [18,19]. In Fig. 4a–c, the experimental and the corresponding simulated XRF spectra of these soil particles measured by the LNLS μ-XRF set-up are shown. The agreement between the measured and simulated spectra is satisfactory for these particles; both with respect to the fluorescence line and scatter background intensities.

As illustrated in Table 4, the U concentration within these particles range from 0.12 to 18.4%, which represent concentration values averaged over the entire intersection volume between the beam and the particle agglomerate in question. The EPMA results showed that most of the concentrated DU particles were in the 0.8–1.5 μm size range, which were often agglomerated with

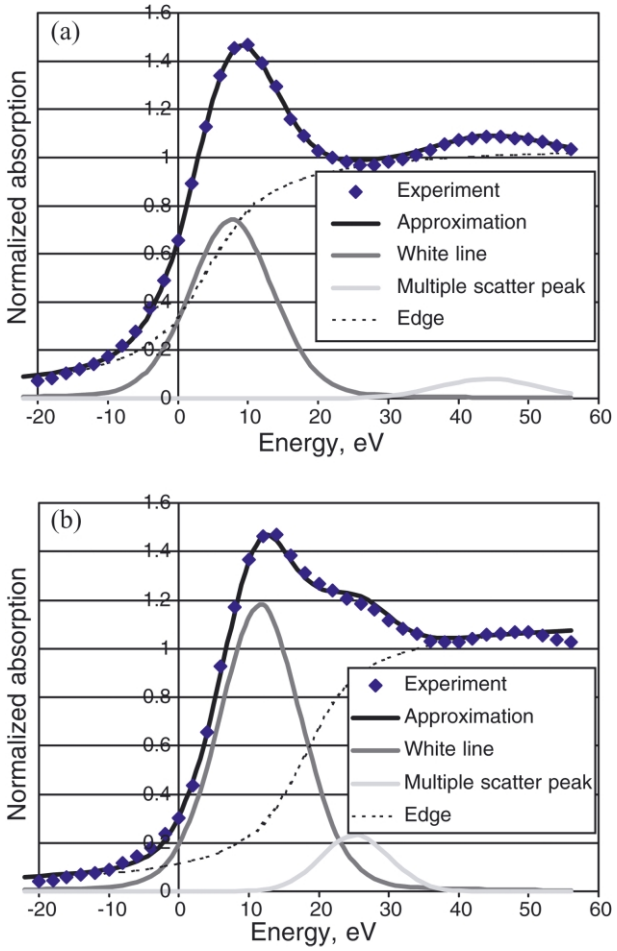

Fig. 5. Least-squares fitting of standard XANES spectra collected at the U L_{III} absorption edge, (a) U(IV) and (b) U(VI) standard. The zero of the energy scale is set to the absorption edge energy of U metal (17 167 eV).

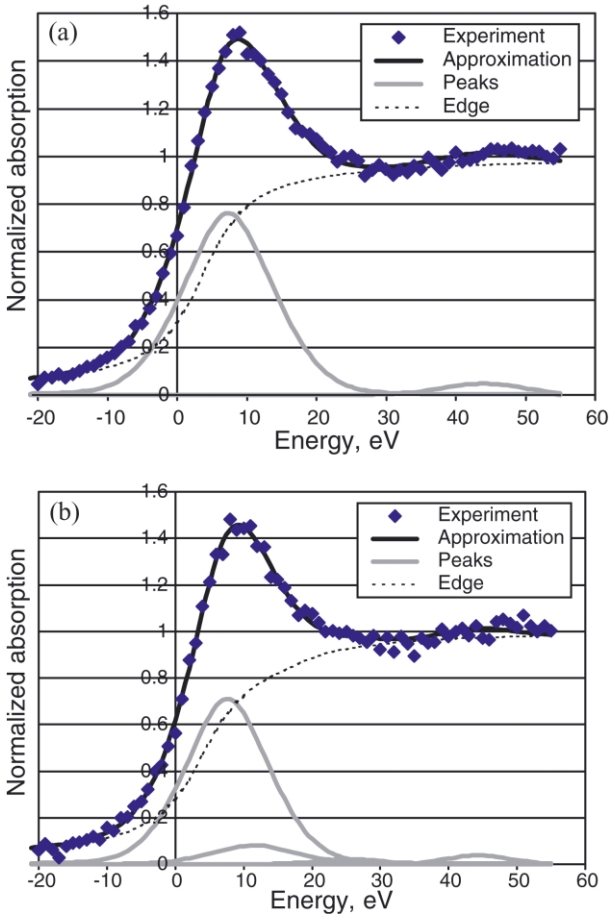

Fig. 6. Examples of least-squares fitting of U XANES spectra of two soil particles collected from Kosovo.

larger soil particles [14]. The particles in the 20–50-μm diameter range were assumed to be heterogeneous, different number of small DU particles were attached to them, therefore the average uranium concentration over the particles could vary in a wide range.

3.5. Micro-XANES results for the Kosovo samples

In order to study the oxidation state of uranium in DU containing soil, μ-XANES spectra were collected on selected individual particles of 20–40-μm diameters. The XANES spectra were processed using a least square fitting method developed by Osán et al. [20] originally for arsenic K-edge absorption spectra. In addition to the

Table 5
Results of least squares fitting of the U-L_{III} XANES spectra of eight individual soil particles collected from Kosovo

	U(IV) (%)	U(VI) (%)	$I_{w(IV)}$	$I_{w(VI)}$	σ_w (eV)	$I_{s(IV)}$	$I_{s(VI)}$	σ_s (eV)	RMS error
Kosovo 1a	100	0	0.887	0.000	7.789	0.081	0.000	19.560	0.029
Kosovo 1b	79	21	0.817	0.222	6.323	0.115	0.158	6.068	0.023
Kosovo 1c	100	0	1.006	0.001	6.550	0.200	0.001	16.620	0.039
Kosovo 1d	100	0	0.977	0.000	6.872	0.137	0.000	17.428	0.054
Kosovo 4a	100	0	0.763	0.000	6.882	0.048	0.000	5.967	0.019
Kosovo 4b	90	10	0.711	0.081	6.363	0.038	0.022	4.656	0.025
Kosovo 4c	92	8	0.736	0.065	6.801	0.072	0.031	5.370	0.031
Kosovo 4d	77	23	0.663	0.200	6.015	0.078	0.121	5.249	0.030

I_w and σ_w: intensity and width of the white line; I_s and σ_s: height and width of the multiple scattering peak; RMS: root mean square. Indices (IV) and (VI) stand for the oxidation state.

measured particulate and thin film standard spectra, fluorescence mode standard spectra of U(IV) and U(VI) measured by Duff et al. [21] at NSLS were also used for the spectrum processing. The energies and intensities of the white line and multiple scattering peak, as well as the parameter of the arctangent step for U(IV) and U(VI) were determined using the standard spectra. The fitting of the standard spectra is demonstrated in Fig. 5. The ratios of the different oxidation state forms in the particles were calculated using these parameters fixed in the fitting function. Fig. 6 shows two examples of the least squares fitting of the XANES spectra of individual particles recorded at the U L_{III} edge.

Table 5 summarizes the fitting results obtained for eight individual soil particles. I_w and σ_w denote the intensity and width of the white line, while I_s and σ_s correspond to the height and width of the multiple scattering peak. The indices (IV) and (VI) are indicating the oxidation state. The table indicates that uranium is present in the particles mostly in the U(IV) form, the maximum ratio of U(VI) to the total U content was obtained as 24% indicating that the particle contained mainly the less mobile form of U.

Salbu et al. [22] also analyzed DU particles from Kosovo using micro-XANES. Based on the results for 12 particles, the authors claimed that approximately 50% of the DU particles were in the form of UO_2, while the remaining DU particles were U_3O_8 or a mixture of oxidized forms. However, the number of particles measured was statistically insufficient to draw relevant environmental conclusions. Although U as only U_3O_8 were not observed in the particles investigated in the present research, the results are not statistically different from that presented by Salbu et al. As it was previously discussed [20] the least-squares fitting of the near-edge features is superior for oxidation state determination than the inflection point energy shift.

The measurements performed on these particles showed that the techniques employed are suitable for the determination of the oxidation state of uranium in microparticles. The results indicate that even though the uranium is mainly present in the oxidation state (IV), still a small fraction is found at the oxidation state (VI), which might contribute in mobilization of uranium in the environment. As a comparison, Duff et al. [21] observed that 75% of the uranium was present as U(VI) in evaporation basin sediments, indicating the difference of the source and weathering conditions of uranium.

4. Conclusions

The automatic SEM screening method is a powerful tool to localize, identify and characterize particles containing uranium present in soil samples in terms of size distribution and elemental chemical composition. For most of the particles found in the soil samples stemming from Kosovo, an average size of approximately 1 μm was measured, which is in agreement with the value reported by other authors. The applied atomic number and mass-specific methods delivered complementary information; they enabled identification of the source as well as the determination of environmental fate and leachability. In addition, the elemental composition revealed the presence of Ti and Al, which are peculiar components of the penetrator and its cladding, respectively. The uranium isotopic composition measured by SIMS indicates clearly that the particles contained depleted uranium. The presence of traces of ^{236}U was evident, however, exact quantification of this isotope is hindered by a high measurement uncertainty. Micro-XANES analysis on the same particles revealed that the U particles originating from the war heads that remained after several years in the polluted soil are mostly in non-leachable oxidation state IV. In this paper, a combination of methods provides complementary information and is advantageously applied to characterize environmental samples. Particularly, when the radiological hazard depends on the speciation of the pollutants, a detailed characterization of those radioactive particles is essential in view of potential uptake and metabolism and related retention time in the body.

Acknowledgments

The present research was partially supported by the National Science Foundation (OTKA) through Contract No. T034195 and by the IHP-Contract HPRI-CT-2001-00140 of the European Commission. This work is part of the activity of WP6 ‘Environmental and biomedical analysis’ of the CMRC-CE. The János Bolyai Research Fellowship for J. Osán is also appreciated. L. Vincze is the fellow of the Belgian National Foundation for Scientific Research (FWO). The authors acknowledge UNEP and IAEA Analytical Laboratories at Seibersdorf for providing the samples for this research. The help of the staff at the synchrotron sources (LNLS and HASYLAB) as well as Ms. Szilvia Kugler is also appreciated. Mr F. Bocci and Mr O. Bildstein are acknowledged for SEM and SIMS sample preparation.

References

[1] WISE Uranium Project; http://www.antenna.nl/wise/uranium (11 September 2003).
[2] M. Betti, Civil use of depleted uranium, J. Environ. Radioact. 64 (2003) 113–119.
[3] P.A. Uijt de Haag, R.C. Smetsers, H.W. Witlox, H.W. Krus, A.H. Eisenga, Evaluating the risk from depleted uranium after the Boeing 747-258F crash in Amsterdam 1992, J. Hazard. Mater. 76 (2000) 39–58.
[4] E.I. Hamilton, Depleted uranium DU: a holistic consideration of DU and related matters, Sci. Total Environ. 281 (2001) 5–21.

[5] A. Bleise, P.R. Danesi, W. Burkart, Properties, use and health effects of depleted uranium (DU): a general overview, J. Environ. Radioact. 64 (2003) 93–112.
[6] N.D. Priest, Toxicity of depleted uranium, Lancet 357 (2001) 244–246.
[7] B. Vekemans, K. Janssens, L. Vincze, F. Adams, P. Van Espen, Analysis of X-ray spectra by iterative least squares (AXIL): new developments, X-Ray Spectrom. 23 (1994) 278–285.
[8] I. Bondarenko, B. Treiger, R. Van Grieken, P. Van Espen, IDAS: a Windows based software package for cluster analysis, Spectrochim. Acta Part B 51 (1996) 441–456.
[9] G. Tamborini, The Development of the SIMS Technique for the Analysis of Radionuclide in Microparticles from Environmental Materials, Doctorate Thesis, University of Paris-Sud, Orsay, France, December 1998, (in French).
[10] M. Betti, G. Tamborini, L. Koch, Use of secondary ion mass spectrometry in nuclear forensic analysis for the characterization of plutonium and highly enriched uranium particles, Anal. Chem. 71 (1999) 2616–2622.
[11] N. Erdmann, M. Betti, O. Stetzer, G. Tamborini, J.V. Kratz, N. Trautmann, J. van Geel, Production of monodisperse uranium oxide particles and their characterization by scanning electron microscopy and secondary ion mass spectrometry, Spectrochim. Acta Part B 55 (2000) 1565–1575.
[12] C.A. Perez, M. Radtke, H.J. Sanchez, H. Tolentino, R.T. Neuenshwander, W. Barg, M. Rubio, M.I.S. Bueno, I.M. Raimundo, J.J.R. Rohwedder, Synchrotron radiation X-ray fluorescence at the LNLS: beamline instrumentation and experiments, X-Ray Spectrom. 28 (1999) 320–326.
[13] G. Falkenberg, O. Clauss, A. Swiderski, Th. Tschentscher, Upgrade of the X-ray fluorescence beamline at HASYLAB/DESY, X-Ray Spectrom. 30 (2001) 170–173.
[14] P.R. Danesi, A. Markowicz, E. Chinea-Cano, W. Burkart, B. Salbu, D. Donohue, F. Ruedenauer, M. Hedberg, S. Vogt, P. Zahradnik, A. Ciurapinski, Isotopic composition and origin of uranium and plutonium in selected soil samples collected in Kosovo, J. Environ. Radioact. 64 (2003) 143–154.
[15] L. Vincze, A. Somogyi, J. Osán, B. Vekemans, S. Török, K. Janssens, F. Adams, Quantitative trace-element analysis of individual fly-ash particles by means of micro-XRF, Anal. Chem. 74 (2002) 1128–1135.
[16] L. Vincze, K. Janssens, M.L. Rivers, K.W. Jones, F. Adams, A general Monte Carlo simulation of ED-XRF spectrometers. II: Polarized monochromatic radiation, homogeneous samples, Spectrochim. Acta Part B 50 (1995) 127–147.
[17] L. Vincze, K. Janssens, B. Vekemans, F. Adams, Monte Carlo simulation of X-ray fluorescence spectra: Part 4. Photon scattering at high X-ray energies, Spectrochim. Acta Part B 54 (1999) 1711–1722.
[18] I. Szalóki, J. Osán, C.-U. Ro, R. Van Grieken, Quantitative characterisation of individual aerosol particles by thin-window EPMA combined with iterative simulation, Spectrochim. Acta Part B 55 (2000) 1017–1030.
[19] C.-U. Ro, J. Osán, I. Szalóki, J. de Hoog, A. Worobiec, R. Van Grieken, A Monte Carlo program for quantitative electron-induced X-ray analysis of individual particles, Anal. Chem. (2003) 851–859.
[20] J. Osán, B. Török, S. Török, K.W. Jones, Study of the chemical state of toxic metals during the life cycle of fly ash using X-ray absorption near edge structure, X-Ray Spectrom. 26 (1997) 37–44.
[21] M.C. Duff, D.E. Morris, D.B. Hunter, P.M. Bertsch, Spectroscopic characterization of uranium in evaporation basin sediments, Geochim. Cosmochim. Acta 64 (2000) 1535–1550.
[22] B. Salbu, K. Janssens, O.C. Lind, K. Proost, P.R. Danesi, Oxidation states of uranium in DU particles from Kosovo, J. Environ. Radioact. 64 (2003) 167–173.